European Journal of Mechanics / B Fluids 103 (2024) 136–144

Contents lists available at ScienceDirect

European Journal of Mechanics / B Fluids

journal homepage: www.elsevier.com/locate/ejmflu

Newtonian annular Poiseuille and Couette flows with dynamic wall slip

Meryieme EL Farragui [a,*], Otmane Souhar [a], Georgios C. Georgiou [b]

[a] Department of Mathematics, University of Chouaib Doukkali, El Jadida, Morocco
[b] Department of Mathematics and Statistics, University of Cyprus, Nicosia, Cyprus

ARTICLE INFO

Keywords:
Annular Poiseuille flow
Annular Couette flow
Flow cessation
Navier slip
Dynamic slip

ABSTRACT

Analytical solutions are derived for the cessation of annular Poiseuille and Couette flows of a Newtonian fluid in the presence of dynamic wall slip. We employ linear dynamic slip law involving a slip relaxation parameter, which results in the appearance of the eigenvalue parameters in the boundary conditions and thus leads to distinct Sturm–Liouville problems that differ from their static slip counterparts. The proper orthogonality condition is derived and closed-form analytical solutions are obtained for both flows of interest. Representative results are then presented and discussed. In agreement with previous reports for other flows with dynamic wall slip, the present solutions show that wall slip slows down flow dynamics and this effect becomes more pronounced as the slip-relaxation parameter is increased.

1. Introduction

The classical no-slip boundary condition dictates that fluid particles adjacent to a solid boundary, i.e., a wall, adhere to it, attaining its velocity. However, several experimental studies have demonstrated that the no-slip condition is often violated in many flows of both simple and complex fluids [1,2]. In such a case, the relative velocity of the fluid particles with respect to that of the wall is called slip velocity. Wall slip can have beneficial effects, such as reducing the required pressure drop in microfluidic applications [1,3]. However, it can also cause undesired instabilities in certain industrial flows [4,5]. Moreover, wall slip can affect viscosity measurements in viscometric experiments, resulting in inaccurate rheology data [6]. To account for wall slip, several techniques, such as the Mooney method for capillary rheometers [7] and the techniques proposed by Yoshimura and Prud'homme [8] for circular Couette and parallel disk rheometers, are employed to obtain reliable estimates of rheological parameters.

Wall slip has been the subject of extensive experimental, theoretical, and numerical investigations. The slip velocity generally depends on multiple factors, including the properties of the fluid, flow conditions (such as shear and normal stresses, pressure, temperature), and characteristics of the wall/fluid interface [2,9]. Navier's law [10] assumes a linear relationship between the slip velocity, u_w, and the wall shear stress, τ_w, and incorporates a single material parameter, β, to represent all other contributing effects:

$$u_w = \frac{\tau_w}{\beta} \tag{1}$$

The special case of the no-slip boundary condition is recovered, when the value of β approaches infinity. Eq. (1) is static, which implies that the slip velocity does not depend explicitly on the past behavior of the fluid particles. More complex static slip equations have been proposed, such as the power-law modification of Navier's law, non-monotonic slip equations, and equations that predict slip above a stress threshold [2].

In the present study, the focus is on dynamic slip equations that are applicable to time-dependent flows and incorporate a relaxation time parameter, denoted as λ. The dynamic version of Eq. (1) takes the following form [2]:

$$u_w + \lambda \frac{\partial u_w}{\partial t} = \frac{\tau_w}{\beta} \tag{2}$$

where t is the time. It should be pointed out that in steady-state flows, Eq. (2) is equivalent to the Navier slip Eq. (1). The presence of the relaxation parameter implies that the development of slip velocity depends on the past states of the wall shear stress. Dynamic wall slip has been reviewed by Hatzikirakos [2]; see also [11].

The idea of a dynamic slip equation, i.e., a retarted slip boundary condition was first introduced by Pearson and Petrie [12]. Malkin and Patlazhan [13] note that the 'retarded' slip boundary conditions become relevant at large shear rates, which is also supported by the work of Kazatchkov and Hatzikiriakos [14], who proposed a multimode dynamic slip model along with the Wagner constitutive equation to simulate the stress response in start-up and large-amplitude oscillatory shear experiments on a linear low-density polyethylene. In addition to empirical models, it is worthwhile mentioning that dynamic slip

* Corresponding author.
E-mail addresses: elferragui01@gmail.com (M. EL Farragui), souhar.o@ucd.ac.ma (O. Souhar), georgios@ucy.ac.cy (G.C. Georgiou).

https://doi.org/10.1016/j.euromechflu.2023.10.001
Received 1 July 2023; Received in revised form 16 September 2023; Accepted 2 October 2023
Available online 5 October 2023

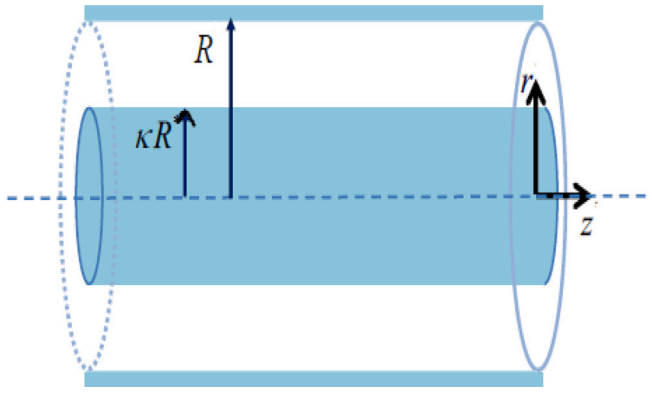

Fig. 1. Geometry of annular Poiseuille flow; the flow is driven by a pressure gradient $G = (-\partial p/\partial z)$.

equations have also been developed using a network kinetic theory combined with Brownian dynamics to simulate the polymer/wall interface [15] and using molecular dynamics simulations to study slip at a solid–fluid boundary [16]. It should be noted that in the latter work, Thalakkottor and Mohseni [16] pointed out that the resulting dynamic slip equation concerned not only gas but also simple liquid flows, i.e., Newtonian flows. More recently, Ebrahimi et al. [17] reported that a dynamic slip equation with a (single) slip relaxation time combined with the K-BKZ viscoelastic constitutive equation is needed to adequately predict the experimental small-angle oscillatory shear and step strain relaxation data on a polydisperse high-density polyethylene melt at large shear deformations. Ebrahimi et al. reported the value $\lambda = 0.224$ s for the slip relaxation time [17].

Kaoullas and Georgiou [11] utilized standard separation of variables to obtain analytical solutions for the start-up and cessation of Newtonian plane and axisymmetric Poiseuille and circular Couette flows with dynamic wall slip. They noted that the eigenvalue parameter appears in the boundary conditions, which produces a Sturm–Liouville problem distinct from that found with the static Navier law, Eq. (1). The primary finding is that dynamic wall slip damps the flow development even more than static wall slip. Similarly, Abou-Dina et al. [18] arrived at equivalent analytical solutions of the start-up Newtonian Couette flow with dynamic wall slip along the fixed wall, using both separation of variables and one-sided Fourier transform methods, and reached the same conclusion.

It is the purpose of this work to derive analytical solutions of the cessation of Newtonian annular Poiseuille and Couette flows in the presence of dynamic wall slip following Eq. (2), which is linear. As demonstrated below, the time-dependence in the boundary condition leads to a more difficult mathematical problem to solve than its static counterpart. The spatial problem is of Sturm–Liouville type where the eigenvalue parameter appears in the boundary condition and thus, the orthogonality condition of the corresponding spatial eigenfunctions must be considered more carefully. In Section 2, we consider the annular Poiseuille flow of a Newtonian fluid with dynamic wall slip. The appropriate orthogonality condition for the spatial eigenfunctions is derived and the full procedure for the solution is given. The implications of the dynamic slip term in the slip equation are then discussed. The annular Couette flow is solved analytically in Section 3. In Section 4, the results for the annular Poiseuille and Couette flow are summarized. Concluding remarks are provided in Section 5.

2. Annular Poiseuille flow

We consider the time-dependent, axial, incompressible, pressure-driven flow of a Newtonian fluid in an infinitely long annular tube of radii κR and R, where $0 < \kappa < 1$ (Fig. 1). We employ cylindrical coordinates (r, θ, z), denote the pressure gradient by $G = (-\partial p/\partial z)$, and assume that gravity is negligible. Under these conditions the z-component of the momentum equation is simplified as follows [19]:

$$\rho \frac{\partial u_z}{\partial t} = G + \eta \frac{1}{r} \frac{\partial}{\partial r} \left(r \frac{\partial u_z}{\partial r} \right), \tag{3}$$

where $u_z = u_z(r, t)$ is the axial velocity, and ρ and η are, respectively, the density and the viscosity of the fluid, both of which are assumed to be constant.

In the present work we assume that wall slip occurs along the two cylinders, i.e., at $r = \kappa R$ and R, following the dynamic slip law given in Eq. (2). Under the above assumptions and noting that the shear stress is positive near the inner cylinder (u_z increases with the radial distance r) and negative near the outer one (u_z is decreasing), one obtains for the two wall shear stresses:

$$\tau_{w1} = |\tau_{rz}|_{r=\kappa R} = \eta \left. \frac{\partial u_z}{\partial r} \right|_{r=\kappa R}, \quad \tau_{w2} = |\tau_{rz}|_{r=R} = -\eta \left. \frac{\partial u_z}{\partial r} \right|_{r=R}. \tag{4}$$

Thus, the boundary conditions at $r = \kappa R$ and R read:

$$\left. \begin{aligned} u_z(\kappa R, t) + \lambda \left. \frac{\partial u_z(r,t)}{\partial t} \right|_{r=\kappa R} &= \frac{\eta}{\beta} \left. \frac{\partial u_z(r,t)}{\partial r} \right|_{r=\kappa R} \\ u_z(R, t) + \lambda \left. \frac{\partial u_z(r,t)}{\partial t} \right|_{r=R} &= -\frac{\eta}{\beta} \left. \frac{\partial u_z(r,t)}{\partial r} \right|_{r=R} \end{aligned} \right\} \tag{5}$$

2.1. Steady-state solution

The steady-state annular Poiseuille flow solution, denoted by $u_z^s(r)$, which serves as the initial condition of the flow cessation, is outlined below. This is easily obtained by integrating the steady-state version of Eq. (3) and applying the static (Navier) boundary conditions

$$\left. \begin{aligned} u_z^s(\kappa R) &= \frac{\eta}{\beta} \left. \frac{du_z^s}{dr} \right|_{r=\kappa R} \\ u_z^s(R) &= -\frac{\eta}{\beta} \left. \frac{du_z^s}{dr} \right|_{r=R} \end{aligned} \right\} \tag{6}$$

If the maximum velocity occurs at $r = \sigma R$, where $\kappa < \sigma < 1$, then $u_z^s(r)$ can be written in the following form [20]:

$$u_z^s(r) = \frac{GR^2}{4\eta} \left[1 + 2(1-\sigma^2) \frac{\eta}{\beta R} - \frac{r^2}{R^2} - 2\sigma^2 \ln\left(\frac{R}{r}\right) \right], \tag{7}$$

where

$$\sigma^2 = \frac{1 - \kappa^2 + 2(1+\kappa)\eta/(\beta R)}{2[\ln(1/\kappa) + (1 + 1/\kappa)\eta/(\beta R)]} \tag{8}$$

It turns out that the slip velocities along the two cylinders are given by

$$u_{w_1}^s = u_z^s(\kappa R) = \frac{GR}{2\kappa\beta}(\sigma^2 - \kappa^2) \tag{9}$$

and

$$u_{w_2}^s = u_z^s(R) = \frac{GR}{2\beta}(1 - \sigma^2). \tag{10}$$

Integrating $u_z^s(r)$ over the annulus cross-section yields the volumetric flow rate

$$Q^s = \frac{\pi G R^4}{8\eta} \left\{ 1 - \kappa^4 + 4(1+\kappa^3)B - \frac{[1 - \kappa^2 + 2(1+\kappa)B]^2}{\ln(1/\kappa) + (1 + 1/\kappa)B} \right\} \tag{11}$$

where

$$B \equiv \frac{\eta}{\beta R} \tag{12}$$

is the dimensionless slip number.

Hereafter, we will work with the dimensionless equations, scaling lengths by R, the velocity by the mean steady-state velocity, $U \equiv Q^s/[\pi(1-\kappa^2)R^2]$, and time by $\rho R^2/\eta$. Dimensionless variables are

denoted by stars. Thus, the dimensionless steady-state velocity is given by

$$u_z^{s*}(r^*) = \frac{2(1-\kappa^2)\left[1+2(1-\sigma^2)B - r^{*2} - 2\sigma^{*2}\ln(1/r^*)\right]}{1-\kappa^4+4(1+\kappa^3)B - \frac{\left[1-\kappa^2+2(1+\kappa)B\right]^2}{\ln(1/\kappa)+(1+1/\kappa)B}}. \tag{13}$$

The no-slip solution is recovered by setting $B = 0$ ($\beta \to \infty$).

2.2. Flow cessation

In this section, we consider the flow cessation assuming that initially ($t^* = 0$) the velocity is the steady-state solution given by Eq. (13), and the pressure gradient suddenly ($t^* > 0$) vanishes. The resulting initial boundary value problem can be written as follows:

$$\left.\begin{aligned}
&\frac{\partial u_z^*}{\partial t^*} = \frac{1}{r^*}\frac{\partial}{\partial r^*}\left(r^*\frac{\partial u_z^*}{\partial r^*}\right), && \kappa \le r^* \le 1, t^* > 0\\
&u_z^*(\kappa,t) + \Lambda\left.\frac{\partial u_z^*(r^*,t^*)}{\partial t^*}\right|_{r^*=\kappa} = B\left.\frac{\partial u_z^*(r^*,t^*)}{\partial r^*}\right|_{r^*=\kappa}, && t^* \ge 0\\
&u_z^*(1,t^*) + \Lambda\left.\frac{\partial u_z^*(r^*,t^*)}{\partial t^*}\right|_{r^*=1} = -B\left.\frac{\partial u_z^*(r^*,t^*)}{\partial r^*}\right|_{r^*=1}, && t^* \ge 0\\
&u_z^*(r^*,0) = u_z^{s*}(r^*), && \kappa \le r^* \le 1
\end{aligned}\right\}, \tag{14}$$

where

$$\Lambda \equiv \frac{\lambda\eta}{\rho R^2} \tag{15}$$

is the dimensionless slip relaxation number.

The above problem is solved using standard separation of variables. Letting

$$u_z^*(r^*,t^*) = X(r^*)T(t^*), \tag{16}$$

substituting into the governing partial differential equation (Eq. $(14)_a$), and separating variables, the solution takes the form

$$u_z^*(r^*,t^*) = \sum_{n=1}^{\infty} A_n X_n(r^*) e^{-\alpha_n^2 t^*}, \tag{17}$$

where $X_n, \alpha_n, n = 1,2,\ldots$ are the admissible eigenfunctions and the corresponding eigenvalues. The eigenfunctions X_n are given by

$$X_n(r^*) = Z_0^n(\alpha_n r^*) \tag{18}$$

as the solutions of

$$\left[r^* X_n'(r^*)\right]' + \alpha_n^2 r^* X_n(r^*) = 0. \tag{19}$$

Here, the functions Z_i^n, $i = 0,1$ are defined by means of

$$Z_i^n(r^*) = J_i(r^*) + \beta_n Y_i(r^*), \quad i = 1,2, \tag{20}$$

where J_i, Y_i are the ith-order Bessel functions of the first and second kind, respectively, and the constants β_n are determined together with α_n by applying the boundary conditions (Eq. $(14)_{b,c}$). One finds that (α_n, β_n) are the solutions of the following algebraic system:

$$\left.\begin{aligned}
&X_n(\kappa)\left(1-\Lambda\alpha_n^2\right) = BX_n'(\kappa)\\
&X_n(1)\left(1-\Lambda\alpha_n^2\right) = -BX_n'(1)
\end{aligned}\right\} \tag{21}$$

or

$$\left.\begin{aligned}
&Z_0^n(\kappa\alpha_n)\left(1-\Lambda\alpha_n^2\right) = -B\alpha_n Z_1^n(\kappa\alpha_n)\\
&Z_0^n(\alpha_n)\left(1-\Lambda\alpha_n^2\right) = B\alpha_n Z_1^n(\alpha_n)
\end{aligned}\right\}. \tag{22}$$

Therefore, the velocity is given by

$$u_z^*(r^*,t^*) = \sum_{n=1}^{\infty} A_n X_n(r^*) e^{-\alpha_n^2 t^*} = \sum_{n=1}^{\infty} A_n Z_0^n(\alpha_n r^*) e^{-\alpha_n^2 t^*}. \tag{23}$$

Once the constants A_n are calculated, all other quantities of interest, such as the two slip velocities, the shear stress τ_{rz}, and the volumetric flow rate Q are easily obtained. For example, the latter two quantities are given by

$$\tau_{rz}^*(r^*,t^*) = \frac{\partial u_z^*}{\partial r^*}(r^*,t^*) = -\sum_{n=1}^{\infty} A_n\alpha_n Z_1^n(\alpha_n r^*) e^{-\alpha_n^2 t^*} \tag{24}$$

and

$$\begin{aligned}
Q^*(t^*) &= \frac{2}{1-\kappa^2}\int_\kappa^1 u_z^*(r^*,t^*) r^* dr^*\\
&= \frac{2}{1-\kappa^2}\sum_{n=1}^{\infty}\frac{A_n}{\alpha_n}\left[Z_1^n(\alpha_n) - \kappa Z_1^n(\alpha_n\kappa)\right] e^{-\alpha_n^2 t^*}.
\end{aligned} \tag{25}$$

The constants A_n are determined by imposing the initial condition (Eq. $(14)_d$) and employing the proper orthogonality condition. In the case of dynamic wall slip ($\Lambda \neq 0$) the resulting Sturm–Liouville problem differs from that for the static case. To derive the proper orthogonality condition, we employ the technique of Anderson and Thomas [11,21]. Multiplying Eq. (19) by X_k, $k = 1,2,\ldots$ and integrating over the interval $(\kappa, 1)$ we have

$$\int_\kappa^1 \left[r^* X_n'(r^*)\right]' X_k(r^*) dr^* + \alpha_n^2 \int_\kappa^1 r^* X_n(r^*) X_k(r^*) dr^* = 0. \tag{26}$$

Integrating the first integral by parts, we obtain

$$\begin{aligned}
&X_n'(1)X_k(1) - \kappa X_n'(\kappa)X_k(\kappa) - \int_\kappa^1 r^* X_n'(r^*)X_k'(r^*)dr^*\\
&\qquad + \alpha_n^2\int_\kappa^1 r^* X_n(r^*)X_k(r^*)dr^* = 0.
\end{aligned} \tag{27}$$

Interchanging n and k and subtracting the resulting equation from Eq. (27) yield:

$$\begin{aligned}
&\left[X_n'(1)X_k(1) - X_k'(1)X_n(1)\right] - \kappa\left[X_n'(\kappa)X_k(\kappa) - X_k'(\kappa)X_n(\kappa)\right]\\
&\quad + (\alpha_n^2 - \alpha_k^2)\int_\kappa^1 r^* X_k(r^*)X_n(r^*)dr^* = 0.
\end{aligned} \tag{28}$$

Substitution of the boundary conditions of Eq. (21) into Eq. (28) yields

$$\begin{aligned}
&(\alpha_n^2 - \alpha_k^2)\left\{\frac{\Lambda}{B}\left[X_n(1)X_k(1) + \kappa X_n(\kappa)X_k(\kappa)\right]\right.\\
&\quad \left. + \int_\kappa^1 r^* X_n(r^*)X_k(r^*)dr^*\right\} = 0.
\end{aligned} \tag{29}$$

The right term of Eq. (29) is not zero only when $k = n$. Its value defines a *norm* of the eigenfunction $X_n(r^*)$, denoted here by N_n:

$$N_n = \frac{\Lambda}{B}\left[X_n^2(1) + \kappa X_n^2(\kappa)\right] + \int_\kappa^1 X_n^2(r^*) r^* dr^*. \tag{30}$$

Therefore, one obtains:

$$\frac{\Lambda}{B}\left[X_n(1)X_k(1) + \kappa X_n(\kappa)X_k(\kappa)\right] + \int_\kappa^1 X_n(r^*)X_k(r^*)r^* dr^* = N_n\delta_{nk}, \tag{31}$$

where δ_{nk} denotes Kronecker's delta. Eq. (31) is the appropriate orthogonality condition for the problem of Eq. (14) [11].

By applying the initial condition (Eq. $(14)_d$), Eq. (17) yields:

$$u_z^{s*}(r^*) = \sum_{n=1}^{\infty} A_n X_n(r^*). \tag{32}$$

Multiplying the above equation by $X_k(r^*)r^*$ and integrating from κ to 1 yields

$$\int_\kappa^1 u_z^{s*}(r^*)X_k(r^*)r^* dr^* = \sum_{n=1}^{\infty} A_n \int_\kappa^1 X_n(r^*)X_k(r^*)r^* dr^*. \tag{33}$$

Multiplying Eq. (32) by $X_k(r^*)$ also leads to

$$f(r^*) = u_z^{s*}(r^*)X_k(r^*) = \sum_{n=1}^{\infty} A_n X_n(r^*)X_k(r^*). \tag{34}$$

Calculating $f(1) + \kappa f(\kappa)$, we obtain:

$$u_z^{s*}(1)X_k(1) + \kappa u_z^{s*}(\kappa)X_k(\kappa) = \sum_{n=1}^{\infty} A_n\left[X_n(1)X_k(1) + \kappa X_n(\kappa)X_k(\kappa)\right]. \tag{35}$$

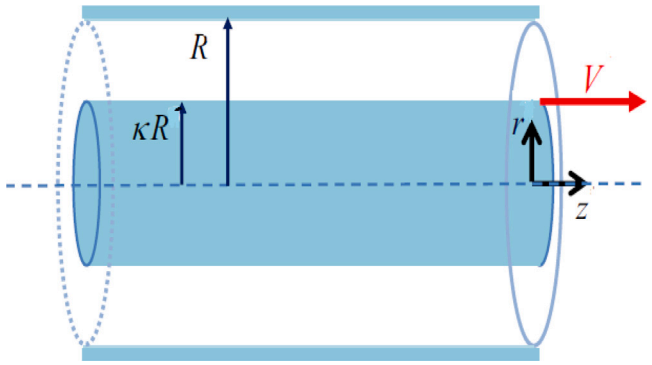

Fig. 2. Geometry of annular Couette flow; the flow is driven by the motion of the inner cylinder.

Adding now the last equation multiplied by Λ/B to Eq. (33), we have

$$\sum_{n=1}^{\infty} A_n \left\{ \frac{\Lambda}{B}\left[X_n(1)X_k(1)+\kappa X_n(\kappa)X_k(\kappa)\right] \int_{\kappa}^{1} X_n(r^*)X_k(r^*)r^*dr^* \right\}$$
$$= \frac{\Lambda}{B}\left[u_z^{s*}(1)X_k(1)+\kappa u_z^{s*}(\kappa)X_k(\kappa)\right] + \int_{\kappa}^{1} u_z^{s*}(r^*)X_k(r^*)r^*dr^*, \tag{36}$$

which, by means of Eqs. (30) and (31), gives

$$A_n = \frac{\frac{\Lambda}{B}\left[u_z^{s*}(1)X_n(1)+\kappa u_z^{s*}(\kappa)X_n(\kappa)\right] + \int_{\kappa}^{1} u_z^{s*}(r^*)X_n(r^*)r^*dr^*}{\frac{\Lambda}{B}\left[X_n^2(1)+\kappa X_n^2(\kappa)\right] + \int_{\kappa}^{1} X_n^2(r^*)r^*dr^*}. \tag{37}$$

Recalling Eq. (18), we have:

$$A_n = \frac{\frac{\Lambda}{B}\left[u_z^{s*}(1)Z_0^n(\alpha_n)+\kappa u_z^{s*}(\kappa)Z_0^n(\alpha_n\kappa)\right] + \int_{\kappa}^{1} u_z^{s*}(r^*)Z_0^n(\alpha_n r^*)r^*dr^*}{\frac{\Lambda}{B}\left[Z_0^{n2}(\alpha_n)+\kappa Z_0^{n2}(\alpha_n\kappa)\right] + \int_{\kappa}^{1} Z_0^{n2}(\alpha_n r^*)r^*dr^*}. \tag{38}$$

After some algebra, one gets:

$$A_n = \frac{4(1-\kappa^2)(1-\Lambda\alpha_n^2)}{\alpha_n^3\left\{1-\kappa^4+4(1+\kappa^3)B-\frac{[1-\kappa^2+(1+\kappa)B]^2}{\ln(1/\kappa)+(1+1/\kappa)B}\right\}} \times \frac{\left\{\begin{array}{c}\Lambda\alpha_n^4\left[2B(1-\sigma^2)Z_1^n(\alpha_n)\right.\\ -\kappa\left\{2B(1-\sigma^2)+1-\kappa^2-2\sigma^2\ln(1/\kappa)\right\}Z_1^n(\kappa\alpha_n)\right]\\ +2(1-\Lambda\alpha_n^2)\left[2+B(1-\sigma^2)\alpha_n^2\right]\left[Z_1^n(\alpha_n)-\kappa Z_1^n(\kappa\alpha_n)\right]\\ \left.-2B\alpha_n^2\left[(1-\sigma^2)Z_1^n(\alpha_n)-(\sigma^2-\kappa^2)Z_1^n(\kappa\alpha_n)\right]\right\}}{\left\{\begin{array}{c}B\alpha_n^2\left[(B+2\Lambda)Z_1^{n2}(\alpha_n)+\kappa(\Lambda-\kappa B)Z_1^{n2}(\kappa\alpha_n)\right]\\ +(1-\Lambda\alpha_n^2)^2\left[Z_1^{n2}(\alpha_n)-\kappa^2 Z_1^{n2}(\kappa\alpha_n)\right]\end{array}\right\}} \tag{39}$$

The special cases for static (Navier) slip ($\Lambda = 0$) and no-slip ($\Lambda = B = 0$) are easily deduced. It should be pointed out, however, that (α_n, β_n) are different, since the eigenvalue problem in Eq. (22) is modified accordingly.

3. Annular Couette flow

We now consider the annular Couette flow, i.e., the flow between two coaxial cylinders of infinite length and radii κR and R, caused by the axial motion of the inner cylinder (see Fig. 2).

3.1. Steady-state solution

The steady-state solution when the pressure gradient is zero and the inner cylinder moves at a constant speed V is easily found by integrating the steady-state version of Eq. (3) and determining the integration constants by imposing the boundary conditions

$$\begin{cases} u_z(\kappa R) = V - u_{w_1} \\ u_z(R) = u_{w_2} \end{cases}, \tag{40}$$

where the two slip velocities, u_{w1}^s and u_{w2}^s, obey the static version of Eq. (2), i.e., the Navier-slip law. Since the velocity is a decreasing function of the radial distance, the shear stress ($\tau_{rz}^s = \eta du_z^s//dr$) is negative everywhere in the flow domain, and thus Eq. (40) takes the form:

$$\begin{cases} u_z^s(\kappa R) = V + \dfrac{\eta}{\beta}\left.\dfrac{du_z^s}{dr}\right|_{r=\kappa R} \\ u_z^s(R) = -\dfrac{\eta}{\beta}\left.\dfrac{du_z^s}{dr}\right|_{r=R} \end{cases}. \tag{41}$$

It turns out that the steady-state velocity and the volumetric flow rate are given by:

$$u_z^s(r) = \frac{B+\ln(R/r)}{(1+1/\kappa)B+\ln(1/\kappa)}V \tag{42}$$

and

$$Q^s = \frac{\pi(1-\kappa^2)R^2V\left[1+2B-2\ln(1/\kappa)/(1/\kappa^2-1)\right]}{2\left[(1+1/\kappa)B+\ln(1/\kappa)\right]}, \tag{43}$$

respectively.

3.2. Flow cessation

Here, we assume that at $t^* = 0$ the velocity is given by the steady-state solution and then, for $t^* > 0$, the inner cylinder stops moving. We work with dimensionless equations, scaling the velocity by the initial speed V of the inner cylinder and lengths and time as in Section 2. The resulting boundary value problem is identical to that in Eq. (14), where now

$$u_z^{s*}(r^*) = \frac{B+\ln(1/r^*)}{(1+1/\kappa)B+\ln(1/\kappa)}. \tag{44}$$

Since the inner cylinder is fixed for $t^* > 0$, the velocity near the inner cylinder increases with the radial distance and thus the signs of the shear stress near the two walls are the same as in the annular Poiseuille flow. Consequently, the resulting eigenvalue problem is also the same (Eq. (22)) and so are the Fourier modes α_n. The dimensionless velocity and volumetric flow rate are given by Eqs. (23) and (25), respectively. Only the constants A_n differ, for which one finds that

$$A_n = \frac{-2\kappa(1-\Lambda)Z_1^n(\kappa\alpha_n)}{\alpha_n\left\{\begin{array}{c}B\alpha_n^2\left[(B+2\Lambda)Z_1^{n2}(\alpha_n)+\kappa(2\Lambda-\kappa B)Z_1^{n2}(\kappa\alpha_n)\right]\\ +(1-\Lambda\alpha_n^2)^2\left[Z_1^{n2}(\alpha_n)-\kappa^2 Z_1^{n2}(\kappa\alpha_n)\right]\end{array}\right\}}. \tag{45}$$

The special cases of Navier slip ($\Lambda = 0$) and no-slip ($\Lambda = B = 0$) are easily recovered from the above general solution.

4. Results and discussion

The Fourier modes corresponding to the analytical solutions derived in this work are easily determined solving the system (22), starting from the first mode, marching along the positive real axis, and calculating all encountered modes till a desired number N is reached. Our numerical experiments revealed that using $N = 1000$ terms of the solution in Eq. (23) was sufficient to ensure series convergence for times greater than 10^{-6}. However, when $t^* < 10^{-6}$, $u_z^*(r^*, t^*)$ does not differ much from the initial steady-state solutions in Eqs. (13) and (44) for the Poiseuille and Couette flows, respectively. Results have been obtained for a range of values of all three flow parameters, i.e., the radii ratio κ, the slip parameter B, and the slip relaxation parameter Λ.

The numerical codes used to compute the analytical solutions have also been checked against the predictions of a naïve fully-explicit finite-difference scheme. As an example, in Fig. 3, the analytical and numerical solutions for both the annular Poiseuille and Couette flows obtained for $\kappa = 0.5$, $B = 0.1$, and $\Lambda = 0.05$ compare quite well. In particular, the solutions for the annular Couette flow (Fig. 3(b)) are indistinguishable at all time steps.

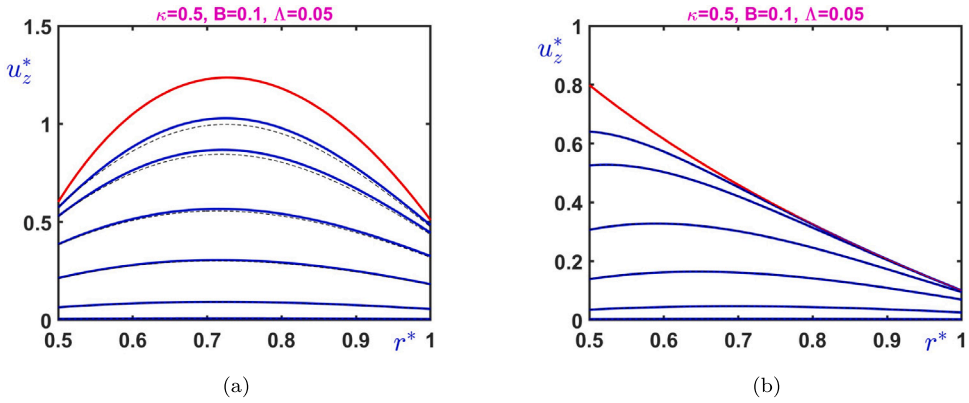

Fig. 3. Comparison of the analytical solutions (solid lines) with the numerical predictions (dashed lines) of a fully-explicit finite difference scheme in the case of cessation of (a) annular Poiseuille flow and (b) Couette flow with dynamic wall slip when $\kappa = 0.5$, $B = 0.1$, and $\Lambda = 0.05$. The velocity profiles at $t^* = 0$, 0.01, 0.02, 0.05, 0.1, 0.2, and 0.4 are shown. The red (top) profiles are the initial steady-state solutions. (For interpretation of the references to color in this figure legend, the reader is referred to the web version of this article.)

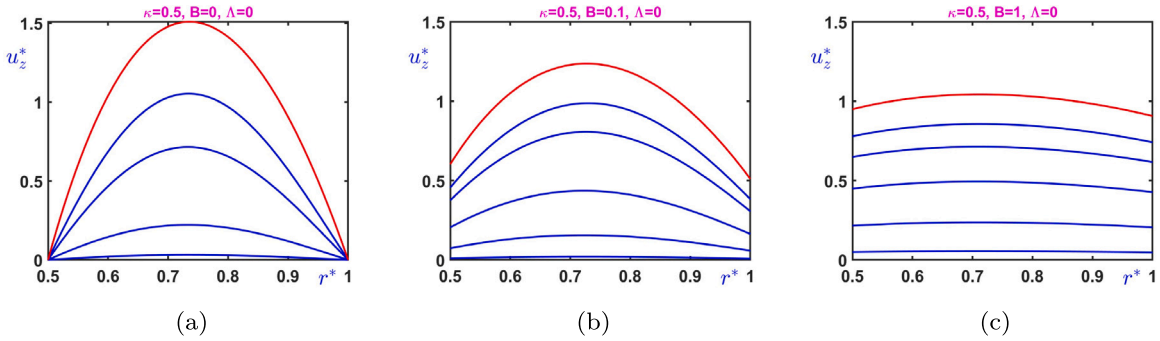

Fig. 4. Evolution of the velocity in cessation of annular Poiseuille flow with Navier slip when $\kappa = 0.5$: (a) $B = 0$ (no slip; $t^* = 0$, 0.01, 0.02, 0.05, 0.1); (b) $B = 0.1$ (moderate slip; $t^* = 0$, 0.01, 0.02, 0.05, 0.1, 0.2); (c) $B = 1$ (strong slip; $t^* = 0$, 0.05, 0.1, 0.2, 0.4, 0.8). The red (top) profile is the initial steady-state solution. (For interpretation of the references to color in this figure legend, the reader is referred to the web version of this article.)

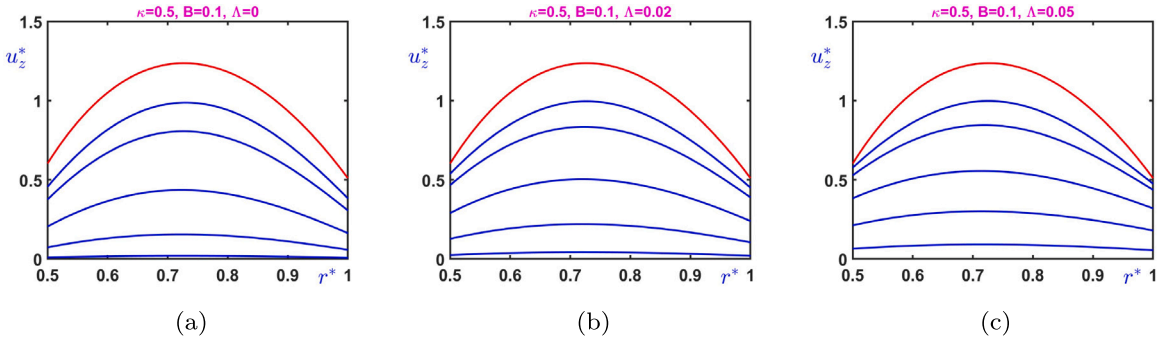

Fig. 5. Evolution of the velocity in cessation of annular Poiseuille flow with dynamic wall slip when $B = 0.1$ (moderate slip) and $\kappa = 0.5$: (a) $\Lambda = 0$ (Navier slip); (b) $\Lambda = 0.02$; (c) $\Lambda = 0.05$. The velocity profiles at $t^* = 0$, 0.01, 0.02, 0.05, 0.1, and 0.2 are shown. The red (top) profile is the initial steady-state solution. (For interpretation of the references to color in this figure legend, the reader is referred to the web version of this article.)

4.1. Annular Poiseuille flow

The evolution of the velocity in the case of Navier slip ($\Lambda = 0$) is first presented for comparison purposes. For this case, it is well known that the velocity profiles tend to become flatter and flow cessation becomes slower, as wall slip becomes stronger [9]. Fig. 4 shows results for the evolution of the velocity, obtained for $\kappa = 0.5$ and three indicative slip numbers corresponding to no ($B = 0$), moderate ($B = 0.1$), and strong ($B = 1$) slip. The effect of the slip relaxation parameter on the evolution of the velocity is illustrated in Figs. 5 and 6, where results with $\Lambda = 0$, 0.02, and 0.05 are shown for $B = 0.1$ and $B = 1$, respectively; Figs. 5a and 6a are thus identical to Figs. 4b and c. In agreement with the literature [9,11,18], the evolution of the velocity becomes slower as Λ is increased. When slip is strong, e.g., in Fig. 6 ($B = 1$), the velocity profiles become rather flat, cessation is much slower, and the effect of Λ is not so pronounced. In other words, dynamic wall slip is not important when slip is very strong.

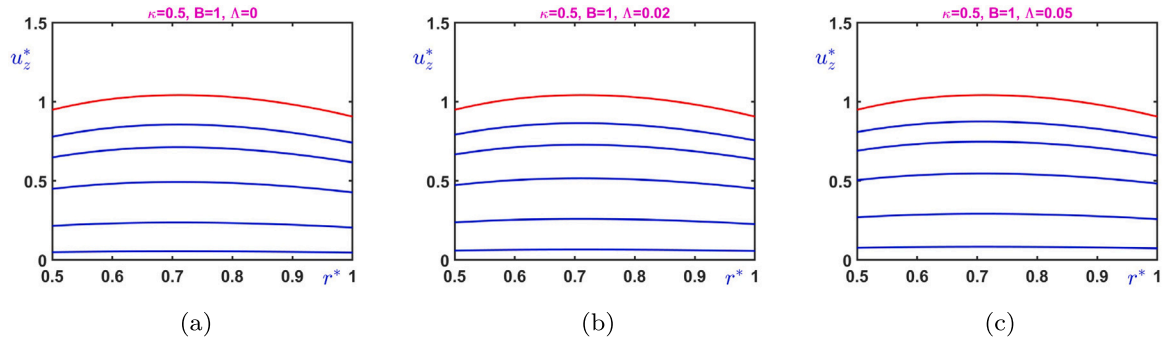

Fig. 6. Evolution of the velocity in cessation of annular Poiseuille flow with dynamic wall slip when $B = 1$ (strong slip) and $\kappa = 0.5$: (a) $\Lambda = 0$ (Navier slip; $t^* = 0, 0.05, 0.1, 0.2, 0.4, 0.8$); (b) $\Lambda = 0.02$ ($t^* = 0, 0.05, 0.1, 0.2, 0.4, 0.8$); (c) $\Lambda = 0.05$ ($t^* = 0, 0.05, 0.1, 0.2, 0.4, 0.8$). The red (top) profile is the initial steady-state solution. (For interpretation of the references to color in this figure legend, the reader is referred to the web version of this article.)

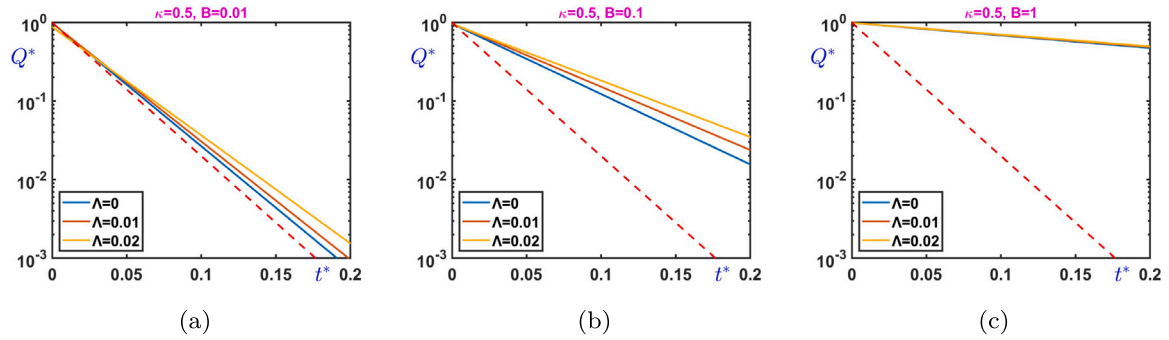

Fig. 7. Evolution of the volumetric flow rate in cessation of annular Poiseuille flow with dynamic wall slip when $\kappa = 0.5$ and $\Lambda = 0$ (Navier slip), 0.01, and 0.02: (a) $B = 0.01$ (weak slip); (b) $B = 0.1$ (moderate slip); (c) $B = 1$ (strong slip). The red dashed line corresponds to the no-slip case.

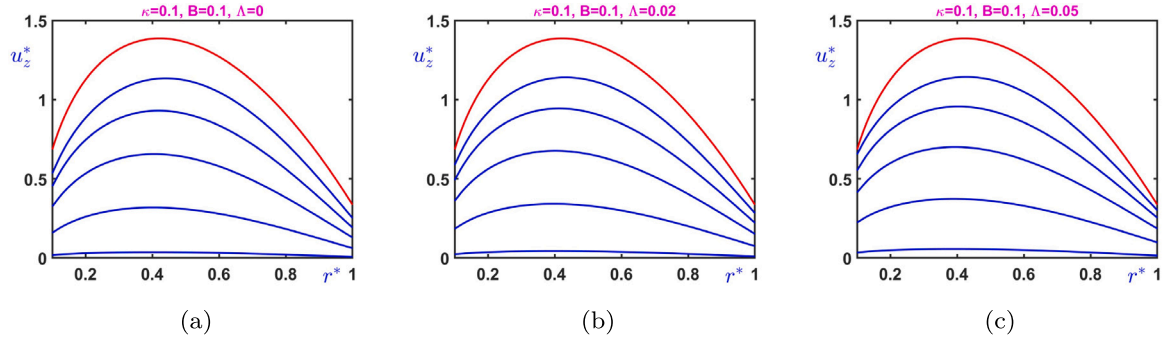

Fig. 8. Evolution of the velocity in cessation of annular Poiseuille flow with dynamic wall slip when $B = 0.1$ (moderate slip) and $\kappa = 0.1$: (a) $\Lambda = 0$ (Navier slip); (b) $\Lambda = 0.02$; (c) $\Lambda = 0.05$. The velocity profiles at $t^* = 0, 0.02, 0.05, 0.1, 0.2$ and 0.5 are shown. The red (top) profile is the initial steady-state solution. (For interpretation of the references to color in this figure legend, the reader is referred to the web version of this article.)

The combined effects of the slip and relaxation numbers on the evolution of the flow are illustrated in Fig. 7, where the calculated volumetric flow rates for different values of the two parameters are plotted. One observes that the evolution of $Q^*(t^*)$ becomes slower when B or Λ are increased and that the effect of Λ is more pronounced when slip is weak (Fig. 7(b)) or moderate (Fig. 7(c)).

The results for other values of the radii ratio κ are quite similar. The damping effect of the slip relaxation parameter on the velocity evolution for $\kappa = 0.1$ and $B = 0.1$ (moderate slip) is shown in Fig. 8 and the combined effects of B and Λ on the volumetric flow rate are illustrated in Fig. 9.

4.2. Annular couette flow

The evolution of the velocity in the case of no or Navier wall slip is illustrated in Fig. 10, where results for $\Lambda = 0$ and $B = 0, 0.1$ and 1 are shown. As expected, the initial steady-state velocity profile tends to become flat and cessation is damped as wall slip becomes stronger. It is also clear that initially only the flow adjacent the inner cylinder of the annular tube is affected. The inner slip velocity u_{w1} is initially much bigger than u_{w2}. As the phenomenon is developed the difference between the two slip velocities diminishes, as they both tend to zero, and the velocity distribution tends to become flatter and more 'symmetric' around $r^* = (1 + \kappa)/2$.

The effect of the slip relaxation parameter is illustrated in Fig. 11, where results for $B = 0.1$ (moderate slip) and different values of Λ are shown. Again, cessation is slowed down and the velocity distribution tends to become flat near the inner cylinder. The evolution of the two slip velocities in the three cases of Fig. 11 is shown in Fig. 12. Since the inner cylinder has stopped and slip velocity is defined as the relative velocity of the fluid with respect to that of the solid boundary, u^*_{w1} is unity initially and decreases more rapidly than u^*_{w2}. The difference

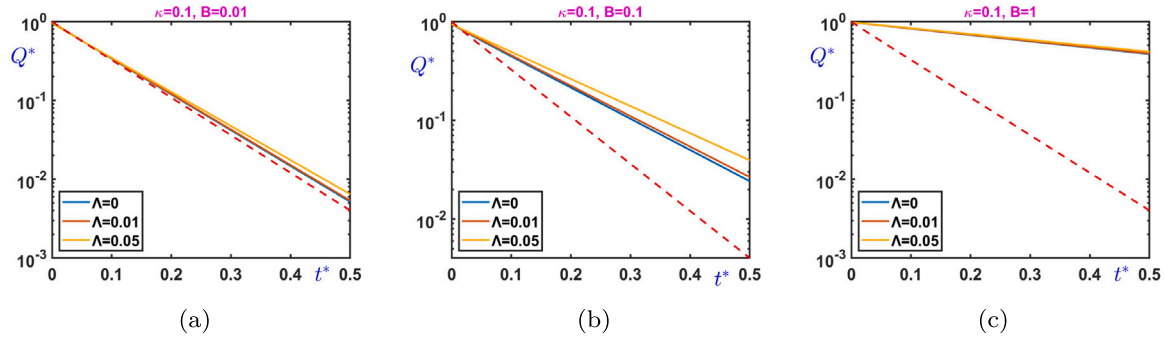

Fig. 9. Evolution of the volumetric flow rate in cessation of annular Poiseuille flow with dynamic wall slip when $\kappa = 0.1$ and $\Lambda = 0$ (Navier slip), 0.01, 0.05: (a) $B = 0.01$ (weak slip); (b) $B = 0.1$ (moderate slip); (c) $B = 1$ (strong slip). The red dashed line corresponds to the no-slip case.

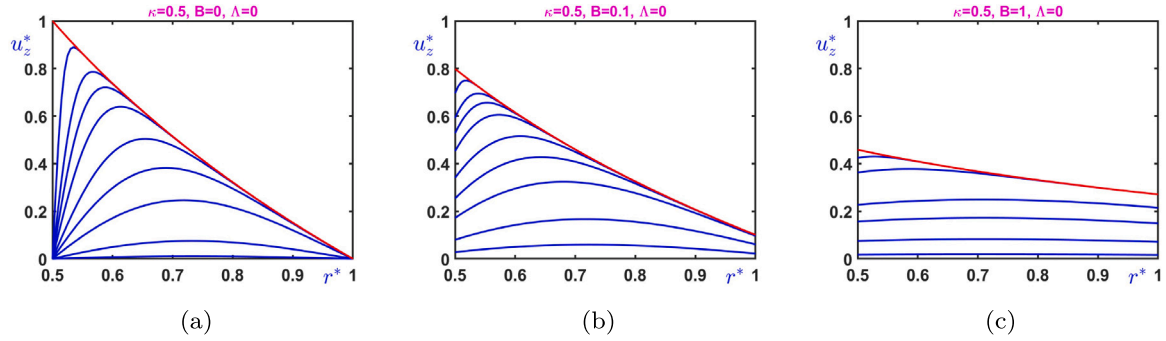

Fig. 10. Evolution of the dimensionless velocity in cessation of annular Couette flow with Navier slip when $\kappa = 0.5$: (a) $B = 0$ (no slip; $t^* = 0$, 0.0001, 0.0005, 0.001, 0.002, 0.005, 0.01, 0.02, 0.05, 0.1); (b) $B = 0.1$ (moderate slip; same times as in (a)); (c) $B = 1$ (strong slip; $t^* = 0$, 0.001, 0.01, 0.1, 0.2, 0.4, 0.8). The red (top) profile is the initial steady-state solution. (For interpretation of the references to color in this figure legend, the reader is referred to the web version of this article.)

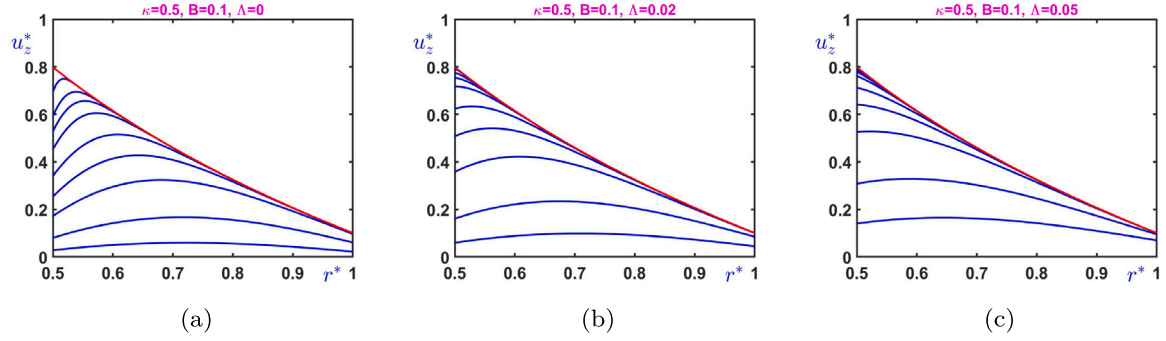

Fig. 11. Evolution of the dimensionless velocity in cessation of annular Couette flow with dynamic wall slip when $\kappa = 0.5$ and $B = 0.1$: (a) $\Lambda = 0$ (Navier slip); (b) $\Lambda = 0.02$; (c) $\Lambda = 0.05$. The velocity profiles at $t^* = 0$, 0.0001, 0.0005, 0.001, 0.002, 0.005, 0.01, 0.02, 0.05, and 0.1 are shown. The red (top) profile is the initial steady-state solution. (For interpretation of the references to color in this figure legend, the reader is referred to the web version of this article.)

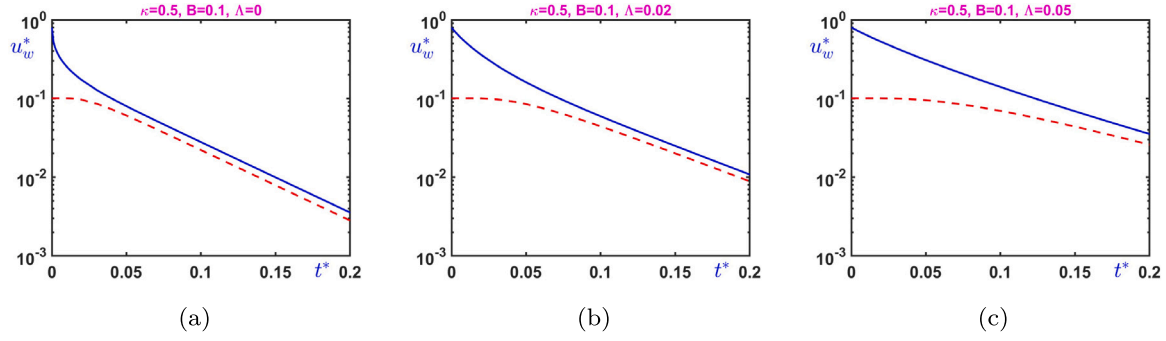

Fig. 12. Evolution of the two slip velocities u^*_{w1} (solid blue) and u^*_{w2} (dashed red) in cessation of annular Couette flow when $\kappa = 0.5$ and $B = 0.1$: (a) $\Lambda = 0$ (Navier slip); (b) $\Lambda = 0.02$; (c) $\Lambda = 0.05$.

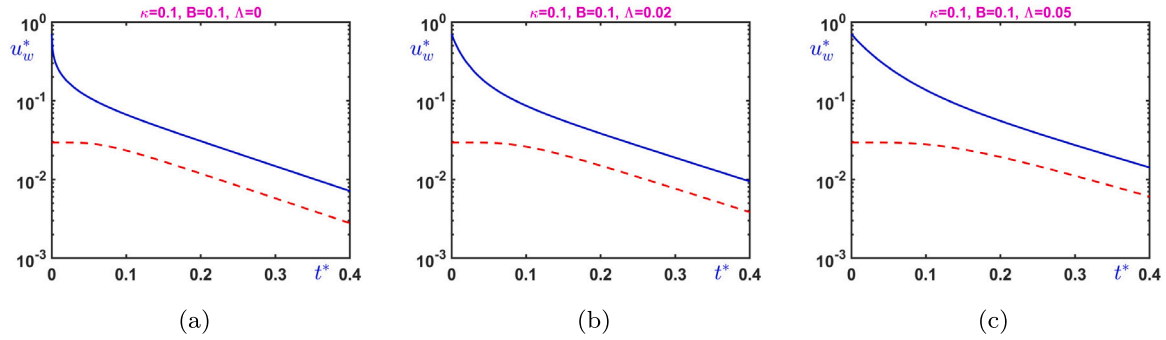

Fig. 13. Evolution of the two slip velocities u_{w1}^* (solid blue) and u_{w2}^* (dashed red) in cessation of annular Couette flow when $\kappa = 0.1$ and $B = 0.1$: (a) $\Lambda = 0$ (Navier slip); (b) $\Lambda = 0.02$; (c) $\Lambda = 0.05$.

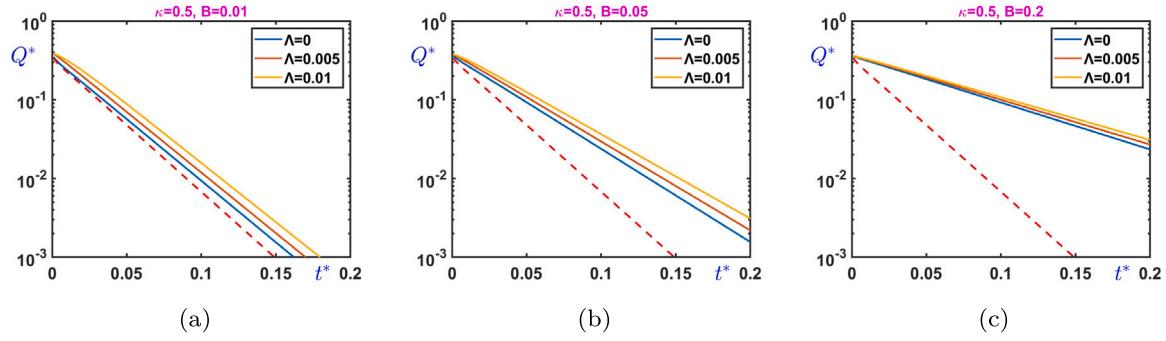

Fig. 14. Evolution of the dimensionless volumetric flow rate in cessation of annular Couette flow with dynamic wall slip when $\kappa = 0.5$ and $\Lambda = 0$ (Navier slip), 0.005, 0.01: (a) $B = 0.01$ (weak slip); (b) $B = 0.1$ (moderate slip); (c) $B = 1$ (strong slip). The red dashed line corresponds to the no-slip case.

between the two slip velocities eventually diminishes as they both decay to zero. The merging of the two slip velocities becomes slower when κ is small, as in Fig. 13, where results for $\kappa = 0.1$ and $B = 0.1$ are shown.

Finally, the evolution of the volumetric flow rate for $\kappa = 0.5$ and various values of B and Λ is shown in Fig. 14. It can be observed that effect of the relaxation parameter is important only when slip is weak or moderate.

5. Conclusion

Analytical solutions have been developed for the cessation of annular Poiseuille and Couette flows of a Newtonian fluid with dynamic wall slip. The solutions show that assuming the same slip law applies along both cylinders of the annulus, the two solutions share the same Fourier modes, with the only difference being in the initial condition. Results for radii ratios $\kappa = 0.5$ and $\kappa = 0.1$ demonstrate that cessation is damped by the slip and relaxation parameters, consistent with previous studies in the literature for other flows [11,18]. It has also been shown that the effect of the slip relaxation parameter is insignificant when slip is strong.

Declaration of competing interest

The authors declare that they have no known competing financial interests or personal relationships that could have appeared to influence the work reported in this paper.

Data availability

No data was used for the research described in the article

Acknowledgment

We are grateful to the anonymous reviewer whose comments led to many improvements of the article.

References

[1] C. Neto, D.R. Evans, E. Bonaccurso, H.J. Butt, V.S.J. Craig, Boundary slip in Newtonian liquids: a review of experimental studies, Rep. Progr. Phys. 68 (2005) 2859–2897.
[2] S.G. Hatzikiriakos, Wall slip of molten polymers, Prog. Polym. Sci. 37 (2012) 624–643.
[3] H.A. Stone, A.D. Stroock, A. Ajdari, Engineering flows in small devices: microfluidics toward a lab-on-a-chip, Annu. Rev. Fluid Mech. 36 (2004) 381–411.
[4] M.M. Denn, Extrusion instabilities and wall slip, Annu. Rev. Fluid Mech. 33 (2001) 265–287.
[5] G. Georgiou, Stick–slip instability. Chapter 6, in: S.G. Hatzikiriakos, K. Migler (Eds.), Polymer Processing Instabilities: Control and Understandlng, Mercel Dekker, Inc., 2004, pp. 161–206.
[6] A.A. Moud, J. Piette, M. Danesh, G.C. Georgiou, S.G. Hatzikiriakos, Apparent slip in colloidal suspensions, J. Rheol. 66 (1) (2022) 79–90.
[7] M. Mooney, Explicit formulas for slip and fluidity, J. Rheol. 2 (1931) 210–222.
[8] A. Yoshimura, A.K. Prud'homme, Wall slip corrections for couette and parallel disk viscometers, J. Rheol. 32 (1988) 53–67.
[9] S.G. Hatzikiriakos, Slip mechanisms in complex fluids, Soft Matter 11 (2015) 7851–7856.
[10] C.L.M.H. Navier, Sur les lois du mouvement des fluids, Mem. Acad. R. Sci. Inst. Fr. 6 (1827) 389–440.
[11] G. Kaoullas, G.C. Georgiou, Start-up Newtonian poiseuille and couette flows with dynamic wall slip, Meccanica 50 (2015) 1747–1760.
[12] J.R.A. Pearson, C.J.S. Petrie, On melt flow instability of extruded polymers, in: R.E. Wetton, R.E. Whorlow (Eds.), Polymer Systems: Deformation and Flow, Macmillan, 1968, pp. 163–187.
[13] A.Y. Malkin, S.A. Patlazhan, Wall slip for complex liquids – phenomenon and its causes, Adv. Colloid Interf. Sci. 257 (2018) 42–57.
[14] I.B. Kazatchkov, S.G. Hatzikirakos, Relaxation effects of slip in shear flow of linear molten polymers, Rheol. Acta 49 (2010) 267–274.
[15] S.G. Hatzikiriakos, N. Kalogerakis, A dynamic slip velocity model for moten polymers based on a network kinetic theory, Rheol. Acta 33 (1994) 38–47.

[16] J.J. Thalakkottor, K. Mohseni, Analysis of boundary slip in a flow with an oscillating wall, Phys. Rev. E 87 (2013) 018.
[17] M. Ebrahimi, V.K. Konaganti, S.G. Hatzikiriakos, Dynamic slip of polydisperse linear polymers using partitioned plate, Phys. Fluids 30 (2018) 030601.
[18] M.S. Abou-Dina, M.A. Helal, A. Ghaleb, G. Kaoullas, G.C. Georgiou, Newtonian plane couette flow with dynamic wall slip, Meccanica 55 (2020) 1499–1507.
[19] T. Papanastasiou, G. Georgiou, A. Alexandrou, Viscous Fluid Flow, CRC Press, Boca Raton, 2000.
[20] E. Gryparis, G.C. Georgiou, Annular poiseuille flow of bingham fluids with wall slip, Phys. Fluids 34 (2022) 033103.
[21] G.L. Anderson, C.R. Thomas, A forced vibration problem involving time derivatives in the boundary conditions, J. Sound Vib. 14 (2) (1971) 193–214.